

Document downloaded from:

<http://hdl.handle.net/10251/55787>

This paper must be cited as:

Anza Hormigo, S.; Vicente Quiles, CP.; Gil Raga, J.; Mattes, M.; Wolk, D.; Wochner, U.; Boria Esbert, VE... (2012). Prediction of multipactor breakdown for multicarrier applications: the quasi-stationary method. *IEEE Transactions on Microwave Theory and Techniques*. 60(7):2093-2105. doi:10.1109/TMTT.2012.2197021.



The final publication is available at

<http://dx.doi.org/10.1109/TMTT.2012.2197021>

Copyright Institute of Electrical and Electronics Engineers (IEEE)

Additional Information

© 2012 IEEE. Personal use of this material is permitted. Permission from IEEE must be obtained for all other uses, in any current or future media, including reprinting/republishing this material for advertising or promotional purposes, creating new collective works, for resale or redistribution to servers or lists, or reuse of any copyrighted component of this work in other works.

# Prediction of Multipactor Breakdown for Multi-carrier Applications: The Quasi-stationary Method

S. Anza, C. Vicente, *Member, IEEE* J. Gil, *Member, IEEE* M. Mattes, *Member, IEEE* D. Wolk, U. Wochner, V. E. Boria, *Senior Member, IEEE*, B. Gimeno, *Member, IEEE*, D. Raboso

**Abstract**—A new prediction algorithm for multipactor breakdown determination in multi-carrier signals is presented. This new algorithm assumes a quasi-stationary model, based on the nonstationary theory for single-carrier signals. It determines the worst case, i.e the combination of signal phases that yields the lowest breakdown level per carrier, using multipactor electron growth models. It considers the Secondary Emission Yield properties of the material and the time-varying value of the multi-carrier signal envelope.

Several test samples have been designed and manufactured in order to assess the precision of the proposed method. The experimental results show excellent agreement with the predicted results. The quasi-stationary prediction technique yields, in general, better accuracy and more relaxed breakdown levels than the existing methods.

**Index Terms**—Vacuum breakdown, RF signals, Passive circuits.

## I. INTRODUCTION

**M**ULTIPACTOR, also known as multipactoring or multipaction, is an electron avalanche-like discharge occurring in microwave devices operating at high power levels and in vacuum or near vacuum condition [1]–[3]. When initially discovered, it was studied as a beneficial effect for signal amplification in cold-cathode tube for TV applications by P. Farnsworth [4], who originally coined the name of multipactor. Nowadays, multipactor is considered as a dangerous collateral effect in high-power vacuum applications, which must be avoided.

The phenomenon occurs when initial free electrons (primary) are accelerated by the RF fields, and impact against the device walls with enough energy to extract more electrons (secondary) from the surface. If the resulting electronic bunch enters in resonance with the field, this process repeats itself

S. Anza, C. Vicente and J. Gil are with Aurora Software and Testing S.L., Edificio de Desarrollo Empresarial 9B, Universidad Politécnica de Valencia, Camino de Vera s/n, 46022 Valencia, Spain, E-mail: sergio.anza@aurorasat.es

M. Mattes is with the Laboratory of Electromagnetics and Acoustics (LEMA), Ecole Polytechnique Fédérale de Lausanne (EPFL), Station 11, CH-1015 Lausanne, Switzerland

D. Wolk and U. Wochner are with TESAT Spacecom GmbH & Co. KG, Gerberstrasse 49, D-71522 Backnang, Germany

V. E. Boria is with the Departamento de Comunicaciones - iTEAM, Universidad Politécnica de Valencia Camino de Vera s/n, 46022 Valencia, Spain

B. Gimeno is with the Departamento de Física Aplicada y Electromagnetismo - ICMUV, Universitat de València c/ Dr. Moliner, 50, 46100 Valencia, Spain

D. Raboso is with the Payloads Systems Division, European Space Agency, 2200-AG, Noordwijk, The Netherlands

until the electron density reaches a certain level to produce noticeable disturbance of the signal, such as distortion, additive noise or reflection, and ultimately produces a destructive discharge that can even damage the device. Multipactor may appear in many types of components, such as passive or active high power devices in guided or microstrip technologies and antennas. Thus, it affects different industry sectors such as satellite communications [5] or particle accelerators [6].

The biggest effort of the multipactor research lines is devoted to the study and characterization of the phenomenon in order to predict under which conditions it will appear, and thus design multipactor-free components. Traditionally, multipactor has been studied for single-carrier signals. The single-carrier prediction techniques are usually based on the multipactor theory, for which there are abundant references (see for example [1]–[3]), and 2D or 3D numerical Particle-in-cell codes (PIC) [7]–[10], which combine electromagnetic solvers and electron trackers. Given some input parameters, such as the frequency of operation, device dimensions and material Secondary Emission Yield (SEY) properties, these single-carrier prediction methods provide the threshold for the multipactor breakdown power. The predicted thresholds are used by the industry to design and assess the margins of operated power in the device to be multipactor-free.

Nevertheless, realistic satellite communication systems combine more than one channel in a single output, what is called a multi-carrier signal. The multi-carrier signal combines the transmission power of the individual channels. Its amplitude is time varying and depends on the relative amplitudes and phases of the channel carriers. Therefore, in the multi-carrier path of the spacecraft (after multiplexing the channels) extremely high peak power levels may be attained, thus increasing the risk of a multipactor discharge [11], [12].

By the time of speaking, the theory for multipactor and multi-carrier signals is rather scarce. To the authors' knowledge, the only existing full theory for multi-carrier operation is provided in [13]. Numerical solvers capable of handling multi-carrier signals exist as well [8], [14], [15]. However, in the multi-carrier case there are many more parameters involved in the multipactor discharge than for the single-carrier case, which include the carrier frequency spacing, the relative phases among the carriers and the amplitude (or power) per carrier. Therefore, the current multipactor theory and numerical software for multi-carrier signals are able to determine if there is multipactor discharge for a fixed configuration. However, they

do not provide the worst case, which is the combination of all the variables of the problem that produces a multipactor discharge with the minimum power per carrier. Thus, the current multi-carrier theory/software do not predict the lowest multipactor breakdown level.

The design rules that are currently being applied by the space industry are based on simplifications that allow applying the single-carrier predictions to the multi-carrier case. The most restrictive one is the  $K^2$ ,  $K$  being the number of carriers, which takes the peak power of the multi-carrier signal as the CW power of an equivalent single-carrier signal. The multipactor breakdown is then equal to  $P_{sc}/K^2$  per carrier, where  $P_{sc}$  is the single-carrier breakdown that can be calculated with single-carrier predictors [16]. This design rule is known to be very conservative and typically gives much lower breakdown power predictions than measured ones. This poses unnecessary constraints on the design, and usually forces to carry out cumbersome tests campaigns to validate the components.

The first attempt for trying to reduce the margins is the 20-gap-crossing rule (20GCR) [16], [17], which establishes a more relaxed criterion of multipactor: It can only appear when the multi-carrier signal envelope is above the single-carrier threshold for a time such that an electron crosses the gap 20 times. In other words, the 20GCR rule allows the multi-carrier signal to be above the threshold for a short time, assuming that the electron build-up will not be enough to produce a discharge. Equivalently, the above  $K^2$  rule would be the zero-gap-crossing rule, i.e. it does not allow any electron crossing (impact) above the threshold. With respect to the  $K^2$  rule, the 20GCR predicts higher multipactor thresholds and reduces the design constraints.

However, the 20GCR rule is based only on the study of numerical simulations and measurements, and does not have a solid physical basis. The question that naturally arises is why 20 and not another value, and why 20 should be a universal value valid for all kind of signals and devices. This uncertainty on the prediction rule implies large safety margins that are imposed to the predicted values [16]. As a consequence, the 20-gap-crossing rule, although being more relaxed than the  $K^2$  rule, still yields very conservative predictions in most cases.

This work proposes a novel Quasi-Stationary (QS) prediction technique for multipactor in multi-carrier signals, with the aim of giving more accurate predictions in order to reduce the safety margins, avoid unnecessary design constraints and reduce the test campaigns as much as possible. Even if a full multi-carrier theory is already available [13], the new technique presented in this paper is still based on the single-carrier theory, following a similar approach as the previous ones. However, it takes more sophisticated simplifications on the multi-carrier signal. By applying the single-carrier theory, the number of parameters of the problem reduces significantly and allows for more simple and intuitive solutions.

The QS prediction method is based on the non-stationary theory for single-carrier signals [18], which belongs to the family of statistical theories that introduce the randomness of electron emission velocity and angle. In spite of their complexity, the statistical theories have the advantage of matching better the experimental results [18], [19]. Among

the statistical theories, the non-stationary one is able to model both the electron growth and absorption, above and below the multipactor threshold, and it considers both single-surface and double-surface interactions. In addition, it gives analytical expressions for the instantaneous SEY and multipactor order. Therefore, the non-stationary theory becomes the most suitable one for multipactor prediction with multi-carrier signals.

Within this work, a number of samples in waveguide technology has been manufactured and tested in order to assess the prediction accuracy of the new QS tool and the current 20GCR. In Section II some background on multipactor is given including a review of the 20GCR. The QS model is presented in Section III. Section IV gives some details on the manufactured samples and the test set-up. The predictions and experimental results are presented in Section VI. Finally, Section VII offers some conclusions.

## II. BACKGROUND

### A. Multipactor in multi-carrier signal

A multi-carrier signal  $V(t)$ , composed of  $K$  carriers with amplitudes  $V_i$ , angular frequencies  $\omega_i$ , and phases  $\phi_i$ ,  $i = 1, \dots, K$ , has the form

$$V(t) = \sum_{i=1}^K V_i \cos(\omega_i t + \phi_i). \quad (1)$$

According to [13], the expression above can be alternatively expressed as a modulated signal with envelope

$$V_e(t) = \sqrt{\left[ \sum_{i=1}^K V_i \cos(\omega_i t + \phi_i) \right]^2 + \left[ \sum_{i=1}^K V_i \sin(\omega_i t + \phi_i) \right]^2}, \quad (2)$$

The envelope is periodic, and its period  $T$  can be computed by finding the greatest common divisor (gcd) of the differences between the signal frequencies ( $f_i = \omega_i/2\pi$ ) and the lowest one ( $f_1$ ).

$$T = 1/f, \quad f = \text{gcd}(f_2 - f_1, f_3 - f_1, \dots, f_K - f_1) \quad (3)$$

For a multi-carrier signal with a specific set of frequencies, its envelope will have a fixed period, but its shape will vary in accordance with the choice of the phase and amplitude of each carrier. The shape may be seen as a set of periodic lobes. In general, the height of such lobes is related to its width in such a way that the higher the envelope is, the narrower the lobes are. Theoretically, for equal amplitude,  $V_i = V_0, \forall i$ , the multi-carrier signal envelope is comprised between two limit values,  $KV_0$  corresponding to the in-phase scheme (all carriers have the same relative phase), and  $\sqrt{K}V_0$  for a totally uncorrelated phase scheme (where the lobes spread and overlap to form a flatter envelope). There are different boundary models which relate the height and the width of the envelope, such as Wolk [20] or Angevain [21] boundary functions. These provide the voltage factor  $F_v$ , which relates the boundary level and the level per carrier, for each envelope width,  $\Delta T$

$$V_e(\Delta T) = F_v(\Delta T)V_0 \quad (4)$$

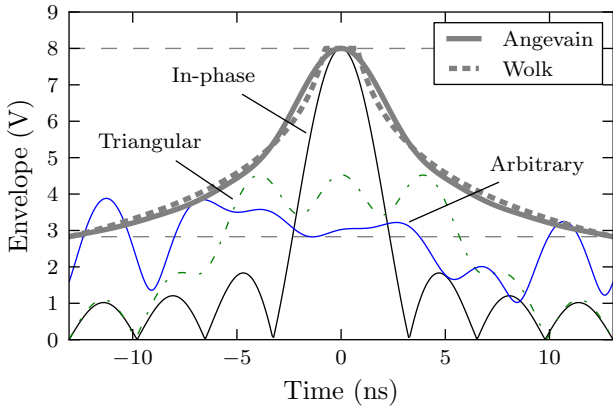


Fig. 1. Multi-carrier signal envelopes for different phase schemes with  $K = 8$  and  $V_i = V_0 = 1$ ,  $\forall i$  with a uniform frequency spacing  $\Delta f = 40$  MHz. Angevain's and Wolk's boundary functions are also plotted.  $KV_0$  and  $\sqrt{K}V_0$  limits are represented by dotted horizontal lines.

Fig.1 shows an example for different phase schemes for a signal with  $K = 8$  and  $V_0 = 1$  with a uniform frequency spacing  $\Delta f = f_{i+1} - f_i = 40$  MHz,  $\forall i$ .

As it is explained in [13] the instantaneous frequency is also periodic with the same period of the envelope, and with an oscillating value around the mean frequency of all carriers. Therefore, the frequency of the multi-carrier signal can be approximated as a constant value equal to the mean frequency of all carriers, i.e.  $f_m$ .

The study of the multipactor phenomenon in multi-carrier signals is rather more complicated than for the single-carrier case. Conceptually, the process can be described as follows. When the multi-carrier signal envelope,  $V_e(t)$ , surpasses a certain level, the electrons are accelerated with enough energy to initiate a multipactor discharge and, thus, the electron population increases. The value of such a threshold is not well known. However, there are evidences that indicate that it must be close to the breakdown threshold in the single-carrier case,  $V_{SC}$ , for a frequency equal to the mean frequency of all carriers,  $f_m$ , as [18] suggests. On the other hand, when  $V_e(t)$  is below  $V_{SC}$ , the electrons impact on the device walls with low energies resulting in a SEY below one, and the electrons being therefore absorbed.

The intervals in which  $V_e(t)$  is above  $V_{SC}$  are called "on" intervals, and those where it is below are known as "off" intervals [22]. Since the envelope is periodic, "on" and "off" intervals are intercalated indefinitely in time. Hence, there will be a multipactor discharge in two cases: Either the "on" interval is long enough to make the electron population grow to a detectable level in the first period of the envelope, which is called a single-event discharge, or the electron growth during the "on" interval is higher than the electron absorption during the "off" interval. This makes the electron population grow slowly, period after period, culminating in a long-term multipactor discharge [22], [23]. Fig. 2 shows an example of a long-term multipactor discharge with an in-phase multi-carrier signal, extracted from [13]. The long-term discharge build-up is typically in the range of few nanoseconds and

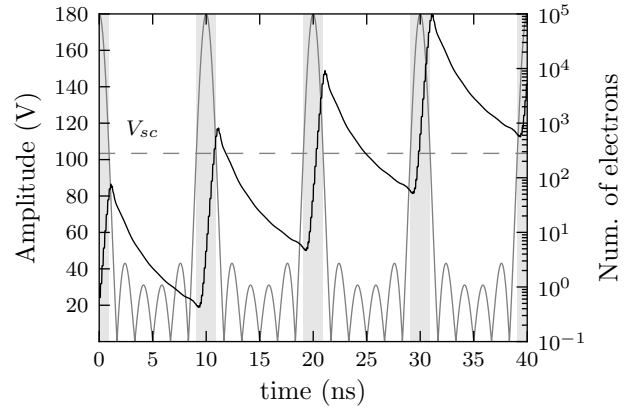


Fig. 2. Example of electron growth in a long-term multipactor discharge extracted from [13], corresponding to a  $K = 6$  carrier signal with equal amplitudes, zero phase (in-phase) and a uniform frequency spacing  $\Delta f = 100$  MHz. Shaded areas correspond to "on" intervals. The single-carrier threshold,  $V_{SC}$  is marked with a horizontal dotted line.

the multipactor discharges are in general not self-sustained. Therefore, in practice, both kind of discharges are indistinguishable in laboratory. Nevertheless, each of them have different implications for the multipactor breakdown level. Long-term discharges are thought to be more restrictive than single-event ones [14], [23].

There are infinite combinations of amplitude and phases that lead to a multipactor discharge. Assuming that all carriers have equal amplitude, the worst case is defined as *the combination of phases that causes a multipactor discharge with the minimum amplitude (or power) per carrier*. This worst case must be the goal of any multipactor prediction method for multi-carrier signals.

### B. The 20-gap-crossing rule

The 20-gap-crossing rule (20GCR) is very simple. It simplifies the multi-carrier envelope as a pulsed signal which can only be above ("on") or below ("off") the single-carrier threshold,  $V_{sc}$ . As its own name indicates, it establishes that there will be a multipactor discharge when the "on" interval is long enough to ensure at least 20 electron impacts [16]. In order to provide a larger margin, the 20GCR takes the lowest frequency of the train of carriers,  $f_1$  (instead of  $f_m$ ), as the reference frequency for the calculation of the single-carrier breakdown threshold. For a multipactor discharge of order  $n$  (the order of the multipactor discharge sets the number of cycles between consecutive impacts for a single electron), the "on" time is

$$T_{20} = \frac{10n}{f_1}. \quad (5)$$

The rule does not give any value for the worst case phases or RF breakdown power. It just gives the length of the "on" interval. In order to find such combination of phases and power, it is necessary to conform the envelope to the desired shape through numerical optimizers, such as simulated annealing [24] or genetic algorithms [25], which search the right combination of phase and amplitude for each carrier

ensuring  $T_{20}$ . Another possibility is to use boundary functions for the envelope amplitude such as [20], [21], which only estimates the breakdown power.

The main advantage of this rule, i.e. its simplicity, is at the same time its main drawback. It is an empirical rule and the criterion that leads to a number of 20 gap crossings it is not clear, and why such a value is applicable to all situations. This is, it does neither take into account how high the envelope with respect to the single-carrier threshold is, nor the dependence of the multipactor order with voltage, or the kind of material in terms of the SEY curve.

The higher the envelope amplitude, the higher the impact energy is, and thus, the higher the SEY [18]. Therefore, it seems logical that for higher amplitudes the number of necessary impacts to cause a detectable discharge gets lower. For instance, for an amplitude equal to the single carrier threshold, the secondary emission yield is nearly one, which implies no electron growth (and no discharge) at all, no matter how many electron impacts occur.

On the other hand, it also seems logical that the number of gap crossings to create a discharge is different for materials with different SEY curves. For example it would be expectable that the number of gap crossings for gold would be higher than for aluminium, since gold is known to typically have a much lower secondary emission yield [16].

Furthermore, the 20GCR only takes into account single-event discharges and completely disregards long-term discharges.

### C. Parallel-plate geometry

Although theories for more sophisticated geometries are available in the literature, the parallel-plate geometry is the simplest and most representative case for all of them, and will be used for the present analysis.

The parallel-plate model assumes an homogeneous RF electric field between the plates, which allows for equivalent voltage definition. But in real microwave applications the circuit and signal specifications are given in terms of signal power, the fields along the structure varying strongly depending on the particular geometry of the device.

In order to translate between both definitions, one may isolate the critical part of the circuit in which multipactor is expected to occur and compute the *voltage at 1W*,  $V_{1W}$ , by means of network theory (for simple structures) or by numerical integration of the electric field along the gap employing full-wave field solvers such as [8], [10], [26]. Therefore, the voltage at the gap  $V_g$ , given an input power  $P_{in}$  is given by

$$V_g = V_{1W} \sqrt{P_{in}}. \quad (6)$$

Of course, this is an approximation that assumes that the electric field is homogeneous along the gap, which does not occur for most practical situations. However, this is the worst case and it is still a valid and commonly used approximation for a wide range of waveguide and coaxial structures [7], [16], [17], [27].

## III. QUASI-STATIONARY MODEL PREDICTION

The Quasi-Stationary (QS) model follows a completely different approach than the 20GCR. It does not simplify the multi-carrier envelope as a pulsed signal, but models the electron growth considering its real time-varying shape  $V_e(t)$ . The worst case is computed searching the envelope that triggers the multipactor discharge with the lowest breakdown power per carrier among all possible shapes. Therefore, the QS model does not employ the concept of "gap-crossings" any more, since it uses a more general and powerful definition of the envelope.

### A. Theory

The QS model is based on the single carrier non-stationary theory [18]. It assumes that the multi-carrier envelope varies slowly enough to consider that its amplitude,  $V_e(t)$ , is constant during an interval  $\Delta t$ . Hence, the first step is to model the electron growth and absorption during such interval by using the single-carrier theory.

Contrarily to the classical multipactor theory, the QS model uses a more sophisticated scenario which considers random electron emission velocity and non-resonant electron trajectories. Therefore, the electrons follow different paths and impact at different times, with different energies. This scenario is valid for voltages above and below the multipactor threshold, which implies electron growth and absorption, respectively. In this scenario, the electron multiplication can be approximated by [22]

$$\Gamma(t, \Delta t) = \frac{N(t + \Delta t)}{N(t)} \simeq 1 + [\sigma_{avg}(t, \Delta t) - 1] I_{acc}(t, \Delta t), \quad (7)$$

where  $\sigma_{avg}(t, \Delta t)$  is the average SEY from  $t$  to  $t + \Delta t$ .  $I_{acc}(t, \Delta t)$  is the accumulated number of impacts given by

$$I_{acc}(t, \Delta t) = \int_t^{t+\Delta t} \frac{2f dt'}{n_i(t')}, \quad (8)$$

where  $n_i(t)$  is the instantaneous multipactor order. Notice that if  $n_i(t)$  is constant, i.e.  $n_i(t) = n$ , (8) becomes equal to the classical theory expression

$$I_{acc}(\Delta t) = \frac{2f \Delta t}{n}. \quad (9)$$

Note that this is a non-resonant process which may be non-stationary as well. This implies that the above averages are dependent on  $t$ .

The non-stationary multipactor theory of [18] provides useful analytical definitions of the main parameters used for constructing the above  $\sigma_{avg}(t, \Delta t)$  and  $I_{acc}(t, \Delta t)$ . These are summarized in Table I (see [18] for their complete mathematical development).

According to [18], the value of instantaneous SEY,  $\sigma_i(t)$ , becomes stable in time for every voltage above and below the breakdown level. Therefore, it is possible to define a constant  $\sigma_{avg}$ , independent of  $t$  and  $\Delta t$ , as the weighted average of  $\sigma_i(t)$  with respect to  $I(t)$

$$\sigma_{avg}(t, \Delta t) \simeq \sigma_{avg} = \frac{\int_0^\infty \sigma_i(t) I(t) dt}{\int_0^\infty I(t) dt}. \quad (10)$$

TABLE I  
DEFINITIONS OF MULTIPACTOR NON-STATIONARY THEORY [18]

Number of electrons	$N(t)$
Impact rate (electrons /second)	$I(t)$
Instantaneous SEY	$\sigma_i(t)$
Instantaneous order	$n_i(t)$

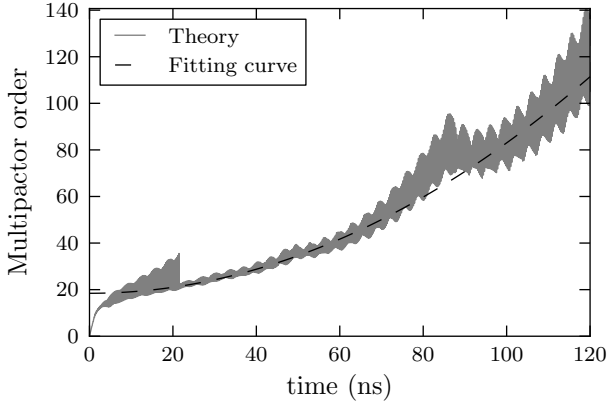


Fig. 3. Fitting of multipactor order. Frequency=3.82 GHz.  $d = 1.3$  mm, silver plating and  $V = 50$  V ( $V_{sc}$  around 361 V). The result is  $\alpha = 6.5 \times 10^{15} s^{-2}$  and  $\beta = 18.43$

Similarly, the value of the instantaneous order  $n_i(t)$  is stable for voltages above the breakdown level and, therefore,  $n_i(t)$  can be approximated as a constant value equal to its weighted average with respect to  $I(t)$ .

$$n_i(t) \simeq n_{avg} = \frac{\int_0^\infty n_i(t)I(t)dt}{\int_0^\infty I(t)dt}. \quad (11)$$

But this is not the case for voltages below breakdown, since the multipactor order diverges increasing indefinitely in time [18]. Since an analytical expression is necessary to derive the rest of the theory, in this work we propose a simple parabolic shape approximation of the form

$$n_i(t) \simeq \alpha t^2 + \beta, \quad (12)$$

which provides a reasonable resemblance with the real behavior. The values of  $\alpha$  and  $\beta$  can be obtained straightforwardly by numerical fitting of the curve. The expression given by (12) is also valid for the region above breakdown ("on" interval), setting  $\alpha = 0$  and  $\beta = n_{avg}$ . Fig. 3 shows an example of such fitting process. Figs. 4, 5 and 6 show detailed maps of the  $\sigma_{avg}$ ,  $\alpha$  and  $\beta$  parameters, respectively, for ECSS silver [16].

Once the electron multiplication is modeled for a single interval  $\Delta t$ , the next step is to model the electron multiplication in the whole period of the multi-carrier envelope.

Note that, in this case the above quantities depend also on the envelope amplitude,

$$\sigma_{avg} \rightarrow \sigma_{avg}(V_e(t)), \quad \alpha \rightarrow \alpha(V_e(t)), \quad \beta \rightarrow \beta(V_e(t)).$$

From now and on  $V_e(t)$  will be omitted from the formulation but its dependence is implied in this model.

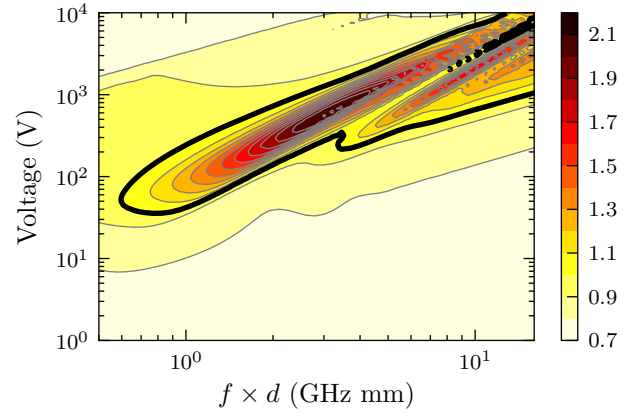


Fig. 4. Multipactor map for average SEY  $\sigma_{avg}$  for ECSS silver [16]

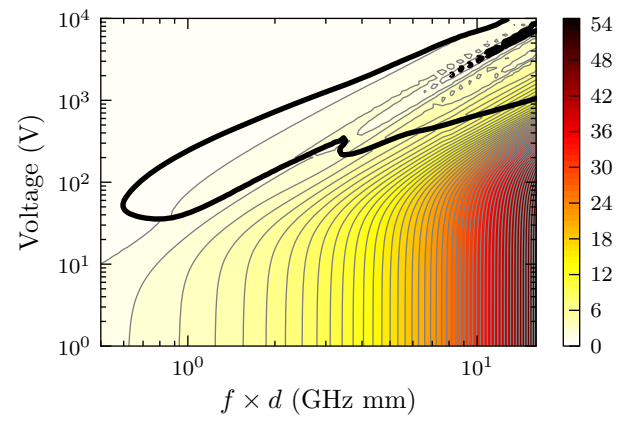


Fig. 5. Multipactor map for  $\beta$  for ECSS silver [16]

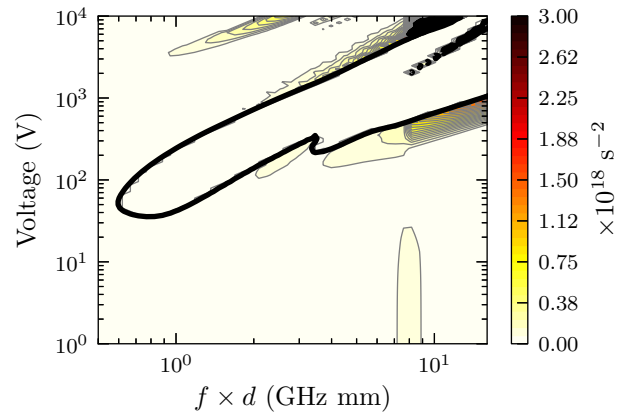


Fig. 6. Multipactor map for  $\alpha$  for ECSS silver [16]

Under such assumptions, the electron multiplication during  $\Delta t$  is

$$\Gamma(t, \Delta t) = 1 + [\sigma_{avg} - 1]I_{acc}(t', \Delta t), \quad (13)$$

The variable  $I_{acc}(t', \Delta t)$  stands for the accumulated electron impacts at time  $t'$  and during an interval  $\Delta t$ , given by

(8).  $I_{acc}(t', \Delta t)$  is dependent on time only during the "off" intervals, where the resonance is lost. Therefore, the reference time  $t'$  corresponds to the time elapsed since the beginning of the last "off" interval.

As stated in (12), the instantaneous order of a multipactor discharge can be considered a constant value in time during the "on" intervals ( $\alpha = 0$ ), and it increases parabolic-like during "off" intervals ( $\alpha \neq 0$ ).

Substituting (12) in (8) and solving the integral

$$I_{acc}(t, \Delta t) = \frac{2f}{\sqrt{\beta\alpha}} \arctan \left[ \sqrt{\frac{\alpha}{\beta}} \frac{\Delta t}{1 + \frac{\alpha}{\beta} t(t + \Delta t)} \right]. \quad (14)$$

Note that during the "on" interval  $\alpha = 0$ ,  $\beta = n_{avg}$ . Then the expression (14) reduces to

$$I_{acc}(t, \Delta t) = \frac{2f\Delta t}{n_{avg}}. \quad (15)$$

Hence, only in the "off" intervals  $\alpha \neq 0$ , implying that  $I_{acc}(t', \Delta t)$  depends on  $t'$ , the time elapsed since the beginning of a particular interval. For an arbitrary multipactor envelope with  $k$  "off" intervals where  $t_{s,i}$  is the starting time, and  $t_{e,i}$  is the ending time for each of them ( $1 \leq i \leq k$ ), the reference time  $t'$  is defined in terms of the absolute time  $t$  as

$$t' = \begin{cases} t - t_{s,1}, & t_{s,1} \leq t < t_{e,1} \\ t - t_{s,2}, & t_{s,2} \leq t < t_{e,2} \\ \dots & \\ t - t_{s,k}, & t_{s,k} \leq t < t_{e,k} \end{cases} \quad (16)$$

Considering a period of the envelope  $T$  with  $l$  divisions such that  $\Delta t = T/l$ , the total electron multiplication for the whole period is

$$\Gamma(T) = \frac{N(T)}{N(0)} = \prod_{i=0}^{l-1} \Gamma(i\Delta t, \Delta t). \quad (17)$$

Finally, the criterion of multipactor is based on a long-term discharge

$$\Gamma(T) \geq 1. \quad (18)$$

The QS model can compute  $\Gamma(T)$  for any multi-carrier envelope.

### B. Procedure for threshold determination

A specific example has been chosen to illustrate the procedure for the threshold determination using the QS model. The example is based on a 6-carrier signal centered at 3.82 GHz with a frequency spacing of  $\Delta f = 100$  MHz and a gap of  $d = 1.31$  mm. The SEY parameters of the Vaughan's model [7] have been chosen as  $W_1 = 29$  eV,  $W_{max} = 399$  eV,  $\sigma_{max} = 2$  and  $\sigma_0 = 0.5$ , for the first cross-over energy, the energy of maximum SEY, the maximum SEY, and the SEY for low electron impact energies, respectively. Fig. 7 shows a diagram with the work-flow of this procedure.

For the specific mean frequency of the multi-carrier signal ( $f_m$ ) and sample gap size of the problem, the  $f \times d$  of operation is derived, for which the SEY,  $\alpha$  and  $\beta$  curves versus signal amplitude are obtained. These curves can be interpolated from precomputed single-carrier maps for the specific SEY

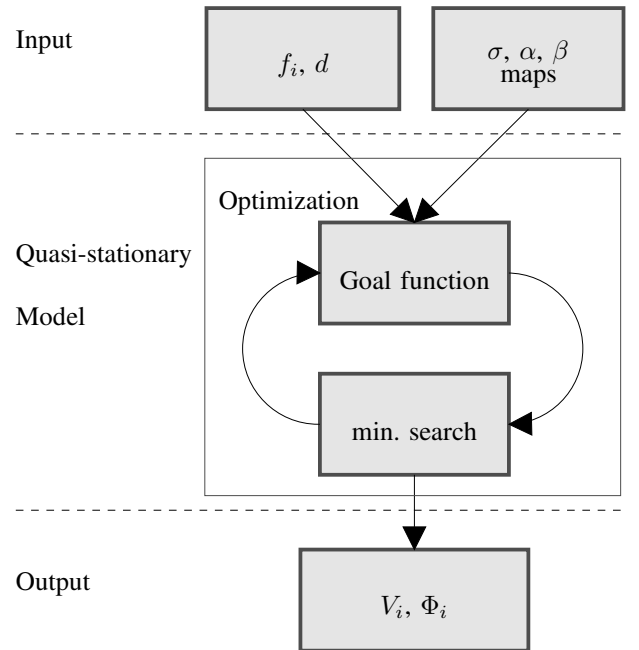


Fig. 7. Quasi-stationary model prediction flow chart.

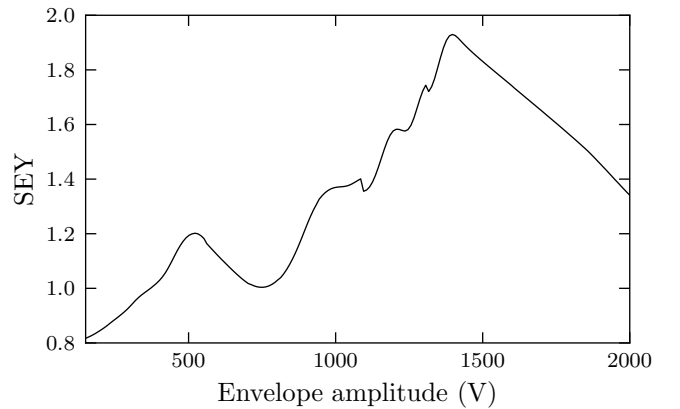


Fig. 8. Curve of SEY versus envelope amplitude,  $V_{on}$ . for  $f \times d = 5.002$  GHz-mm.

parameters of the sample (such as those of Figs. 4-6), or can be ad-hoc computed using the single-carrier non-stationary theory. Figs. 8 and 9 show the  $\alpha$  and  $\beta$  curves for this example. See that  $\alpha = 0$  above the breakdown level (located at 371 V).

With this input data, the QS model is able to approximate the electron growth for any phase distribution and amplitude of the signal carriers. For example, in Fig. 10 the electron growth for a triangular phase scheme and three different values of the amplitude per carrier (equal for all carriers) is shown. These curves are computed with (17) and it is clear that there is electron accumulation ( $\Gamma > 1$ ), and therefore multipactor discharge, for  $V_0 = 142$  V, no discharge ( $\Gamma < 1$ ) for  $V_0 = 125$  V. The breakdown limit ( $\Gamma = 1$ ) is obtained for  $V_0 = 132$  V.

The QS prediction technique uses a global optimizer to search the combination of phases and amplitudes in order to minimize a goal function. Such a goal function must

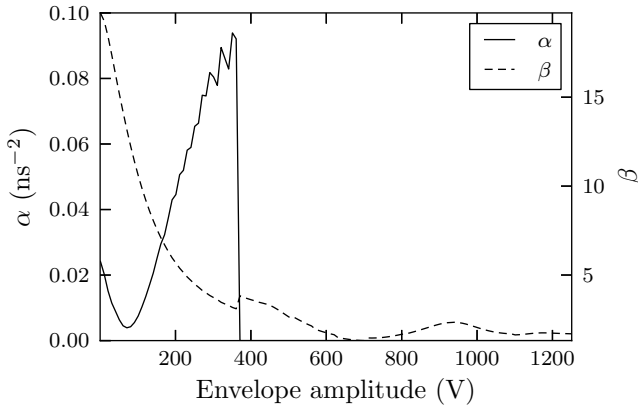


Fig. 9. Curve of  $\alpha$  and  $\beta$  versus envelope amplitude,  $V_{on}$ , for  $f \times d = 5.002$  GHz-mm.

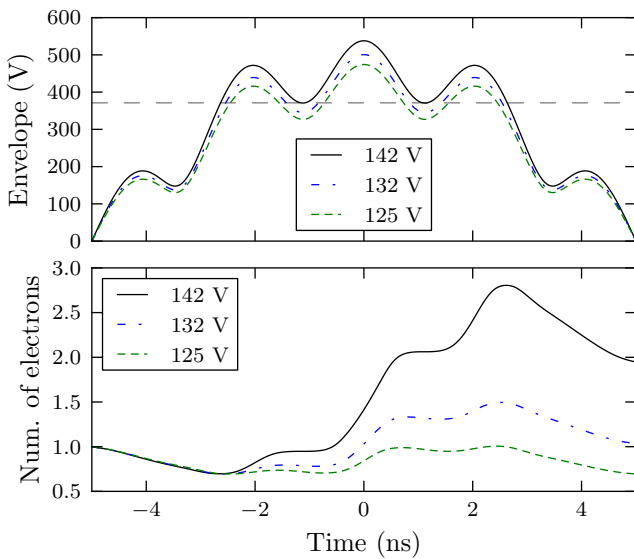


Fig. 10. Electron growth (bottom) according to QS model for different amplitude envelopes of a multi-carrier signal (top). The single-carrier threshold is marked with a horizontal dotted line.

ensure that its minimum corresponds to the worst case. In this example the goal function is

$$G = f(\Gamma) + V_0, \quad (19)$$

where equal amplitude of carriers,  $V_0$ , has been assumed (this method would be also valid for unequal amplitudes).  $\Gamma$  is given by (17), and

$$f(\Gamma) = \begin{cases} w|\Gamma - 1|, & \Gamma < 1 \\ 0, & \Gamma \geq 1 \end{cases}, \quad (20)$$

defines a constraint on the solution, penalizing regions where there is no multipactor ( $\Gamma < 1$ ). No universal values can be provided for the weight  $w$ , which can be tuned to speed up the optimizer or to improve the accuracy of the solution.

The solution of the optimizer (minimizing  $G$ ) is already the worst case for this signal, consisting of the combination of phases that ensures a multipactor discharge for the lowest

TABLE II  
KU-BAND FREQUENCY SCHEME.

#	Channels		Carrier combination			
	freq. (GHz)	BW (MHz)	contiguous		non contiguous	
			6 ch.	8 ch.	6 ch.	8 ch.
1	11.7440	34				x
2	11.8206	34			x	x
3	11.8589	34		x		
4	11.8972	34	x	x	x	x
5	11.9355	34	x	x		
6	11.9738	34	x	x	x	x
7	12.0121	34	x	x		
8	12.0504	34	x	x	x	x
9	12.0887	34	x	x		
10	12.1270	34		x	x	x
11	12.2036	72			x	x
12	12.2802	72				x
$f_m$ (GHz)			11.992		12.012	
$\Delta f$ (MHz)			38.3		76.6	

carrier amplitude. However, keep in mind that the QS model is able to compute other breakdown levels than the lowest one, for any phase and amplitude distribution.

#### IV. TESTING

The objective of the test campaign is to provide meaningful data for different types of situations, such as different gap sizes, number of carriers and carrier phasing, with the aim of demonstrating the correct behavior of the new prediction tool. In order to do so, specific hardware has been manufactured.

##### A. Frequency plans and tests

The frequency plan has been chosen to be in the Ku-band. In order to use different frequency schemes, 4 different signals have been tested: 6 carriers and 8 carriers with contiguous and non-contiguous schemes. A 15-channel Ku-band manifold output multiplexer has been selected for this purpose. The frequency plan of this multiplexer is given in Table II.

8 power amplifiers were available, providing an equivalent peak power level of about 19000 W.

##### B. Sample Design

A total number of 7 Ku-Band waveguide samples have been designed and manufactured with WR 75 interfaces (see Table III).

The gaps of the samples have been selected in order to guarantee that the multipactor mode order is relatively low, and that no change of mode order will occur over the bandwidth of the sample.

The samples have been designed to be as simple as possible, and to avoid effects that may lead to a distortion of the results (e.g. no screws have been used for filter tuning and fringing field effects have been minimized).

Three different kinds of samples have been selected:

- Waveguide with reduced height and transformers on both ends (TF).
- Corrugated lowpass filter (LP).
- Narrow-band bandpass filter with inductive irises and reduced height (BP).



TABLE III  
SAMPLES FOR KU-BAND TESTS.

Type	Gap (mm)	$V_{1W}$ (V)	freq. scheme	$f_m$ (GHz)	$f \times d$ (GHz-mm)	$n$
TF	0.14	3.89	cont.	11.99	1.68	1
			non cont.	12.01	1.68	1
	0.42	8.88	cont.	11.99	5.04	3
			non cont.	12.01	5.05	3
	0.64	10.38	cont.	11.99	7.67	5
			non cont.	12.01	7.69	5
LP	0.14	6.35	cont.	11.99	1.68	1
			non cont.	12.01	1.68	1
	0.42	9.14	cont.	11.99	5.04	3
			non cont.	12.01	5.05	3
	0.64	11.5	cont.	11.99	7.67	5
			non cont.	12.01	7.69	5
BP	1.31	32.1	cont.	11.99	15.71	7
			non cont.	12.01	15.74	7

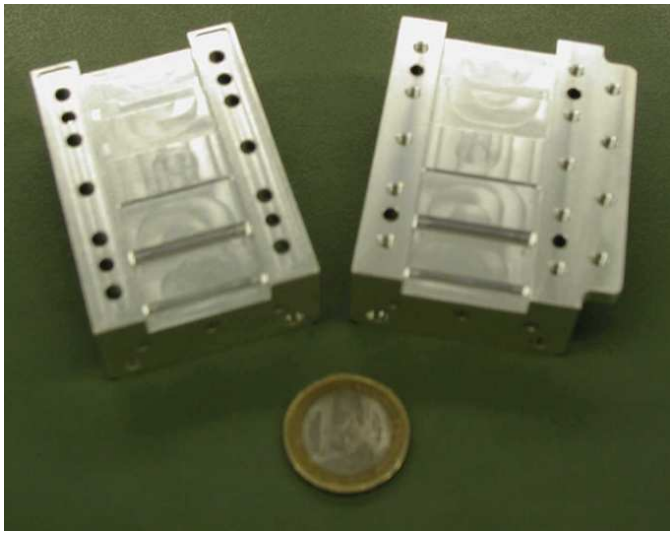


Fig. 11. Ku-band transformer sample.

All samples have been built up in a two-shell configuration. The units are provided with silver plated surfaces. Fig. 11 shows a picture of a Ku-band transformer sample.

### C. Description of the test bed

The schematic of the test set-up is shown in Fig. 12.

The tests have been performed at ambient temperature (24°C). The chamber pressure was below 1 mPa, before starting the multipactor tests.

For the multi-carrier test signal generation, the power of 6 to 8 amplified channels have been combined with a multiplexer. For a steady multi-carrier signal, the phase relation between the single channels has been monitored and adjusted by a phase control unit (computer controlled unit).

Different techniques have been used to detect the occurrence of multipaction:

- 1) Input reflection nulling.
- 2) Near band noise.
- 3) Fast diode detector for near band noise.
- 4) 3rd harmonic.

TABLE IV

SEY PARAMETERS FOR THE KU-BAND SAMPLES. THE FIGURES  $W_1$ ,  $W_{max}$ ,  $\sigma_{max}$  AND  $\sigma_0$ , STAND FOR THE FIRST CROSS-OVER ENERGY, THE ENERGY FOR MAXIMUM SEY, THE MAXIMUM SEY AND THE SEY FOR LOW ELECTRON IMPACT ENERGIES, RESPECTIVELY.

Type	Gap (mm)	$W_1$ (eV)	$W_{max}$ (eV)	$\sigma_{max}$	$\sigma_0$
TF	0.14	38	369	1.84	0.5
	0.42	36	378	1.9	0.5
	0.64	30	356	2.23	0.5
LP	0.14	47	403	1.73	0.5
	0.42	32	370	2.1	0.5
	0.64	25	325	2.2	0.5
BP	1.3	25	309	2.2	0.5

### 5) Fast diode detector for 3rd harmonic.

An electron gun and a remote controlled radioactive source have been used to provide a sufficient amount of free electrons to start the multipacting discharge.

A picture of the vacuum chamber and the test set-up for a Ku-band sample is shown in Fig. 13.

### D. SEY measurements

In order to properly characterize the coating material and obtain good multipactor predictions, it was also necessary to measure the SEY of the different devices.

Since the dimensions of the devices were too large to fit inside the vacuum chamber of the SEY test, the measurements were done for silver-plated aluminium alloy samples of  $50 \times 20 \times 1$  mm which were plated in the same bath used with each of the Ku-band manufactured devices.

The measured SEY parameters are given in Table IV. The SEY measurement is done over a spot of only 2 mm diameter and two measurements have been done for each sample. The manufacturing and plating process is identical for all of them, but significant differences can be appreciated. This is probably due to inhomogeneities in the surface which causes local SEY variations, thus implying a relative dependence of the results on the measurement point.

## V. SIMULATION SOFTWARE

The 20GCR and the QS prediction techniques described in sections II-B and III, respectively, have been used to calculate the worst cases of the samples detailed in Section IV-B. The procedure for the threshold determination described in Section III-B has been followed. No extra margins have been applied to any of the prediction methods. The differential evolution algorithm [25] has been employed for the QS optimization and for the 20GCR signal phase conforming.

All worst case signals, predicted by the QS method, have been simulated with FEST3D [8], a software for full-wave electromagnetic analysis and design of passive microwave passive circuits in waveguide technology, which also includes a RF high power module for multipactor analysis under multi-carrier operation.

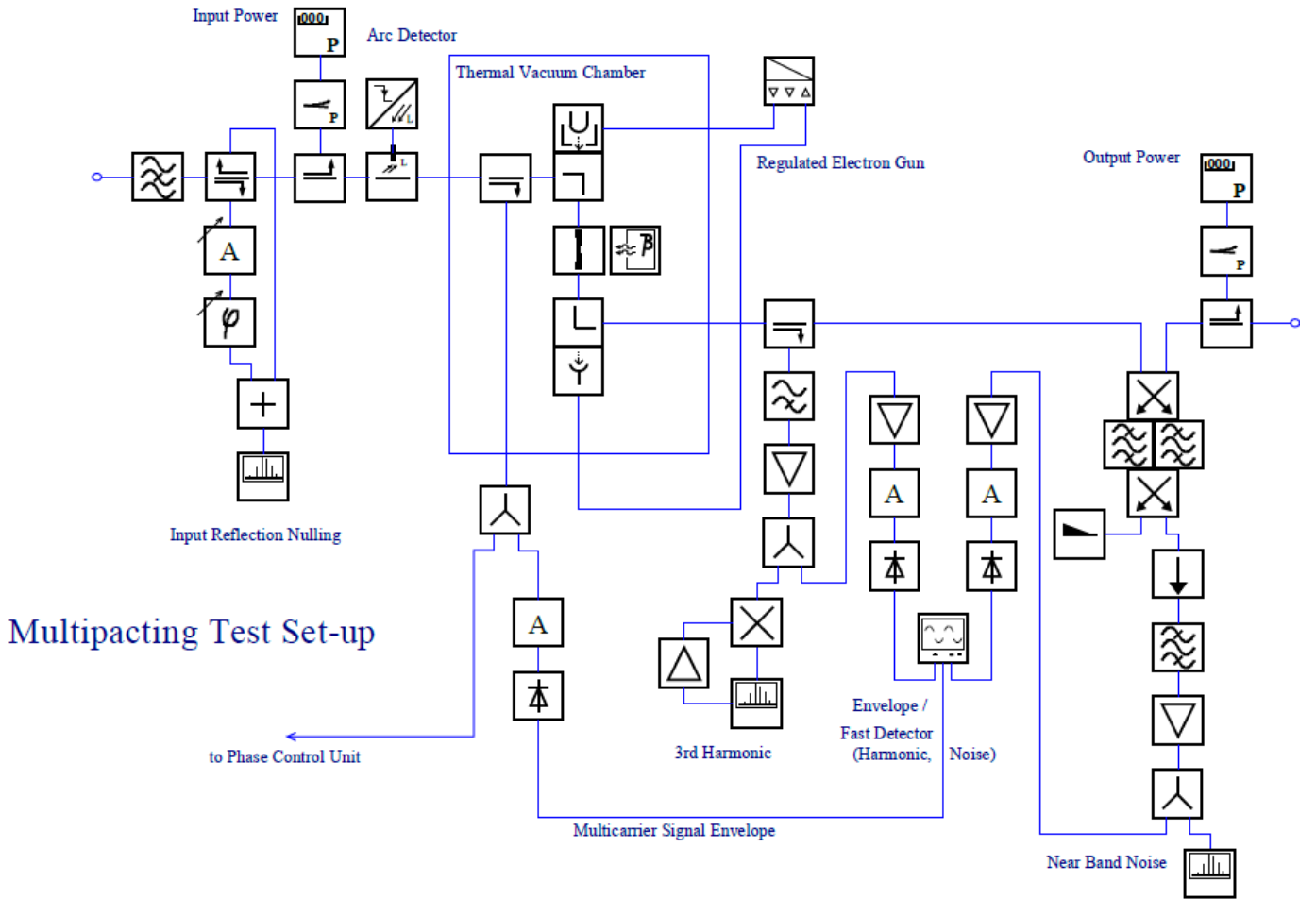


Fig. 12. Schematic for Ku-band test set-up.

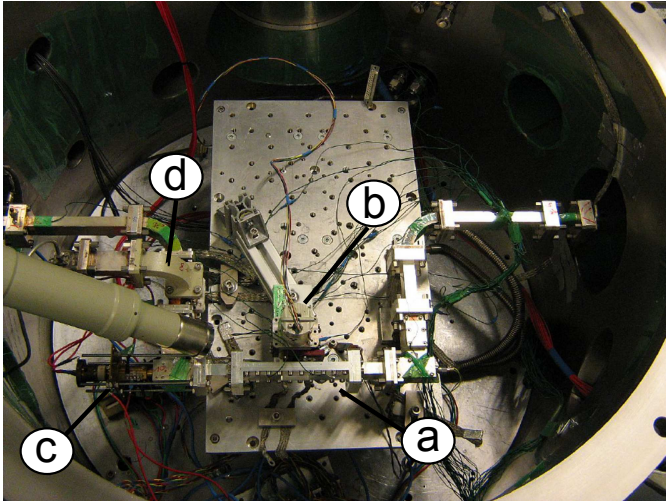


Fig. 13. Ku-band test set-up: Gap sample (a), radioactive source (b), electron gun (c) and coupler for detection of the phase and envelope (d) installed inside the thermal vacuum chamber.

## VI. PREDICTIONS AND TEST RESULTS

### A. Error definition

In our case, the output of the prediction, for a certain multi-carrier signal, is the couple consisting of phase distribution and power per carrier. The purpose of the prediction is to find the worst case, i.e. the combination of phases with the lowest breakdown power. We define:

- Local error: It is defined as the difference between the simulated breakdown power and the experimental one *measured when applying the computed phase distribution*. This error gives an idea of the accuracy of the predictor to correlate the carrier phases and the breakdown power.
- Global error: The global prediction error is defined as the difference between the simulated breakdown power and the *lowest breakdown power of all the tests made with the available phase conditions*. This error measures the capability of predicting the lowest breakdown power.

A predictor that yields a low local error and a high global error, means that it is good to predict the breakdown power of a particular phase distribution, but the optimization of the phases fails to find the lowest breakdown power.

A low global error and high local error means that the predictor apparently is able to find the lowest breakdown power,

but the worst case phase distribution does not correspond to the predicted one. This may happen for some specific cases, but it is unlikely that such a predictor is able to find the lowest breakdown power in a general case.

Finally, a good predictor is one that keeps both errors low.

### B. Phase configurations

Three phase configurations have been used for each test, belonging to the following list:

- In phase (IP): All phases are set to zero.
- QS model (QS): The phases are optimized using the QS method of Section III-B.
- 20-gap-crossing rule (20g): The phases are optimized to comply with the 20-gap-crossing rule worst case phasing, following Section II-B.

The IP phasing has been tested in all samples. In the case that any of the predictions (QS or 20GCR) were equal to the IP phasing, such phase configuration was changed to “free running” phases (FR). In this situation the local oscillators of the amplifiers are left unlocked to the common reference and, hence, their relative phases change randomly. According to the authors’ experience, this kind of test usually yields the lowest breakdown power. Therefore, even if it does not give any information on the envelope or phases, it may be a good reference for computing the global error (see Section VI-A).

Sometimes, not only one but both prediction methods, QS and 20GCR, yielded a solution similar to the IP case. In this case the two phase configurations were changed to FR condition and a non-optimum QS prediction (QSn), i.e., another phase configuration which is not the worst case but for which the QS model can compute a breakdown prediction. This is useful in order to check the QS model prediction local error.

### C. RF breakdown prediction and measurements

Table V shows the predicted worst cases for the two different analytical methods. Labels “c” and “n” stand for contiguous and non-contiguous frequency schemes. Breakdown levels are given in power per carrier. For the 20GCR prediction, a phase optimization has been run to make the envelope match with the desired number of gap crossings. The QS method has been used in order to find the phases that ensures a multipactor discharge with the minimum input power (worst case). The QS method does not employ the number of gap crossings in the optimization procedure. It gives directly the phase distribution. However, the number of gap crossings has been also computed and included in order to compare with the 20GCR.

The predicted breakdown power may be better seen in Fig. 14, where the boundaries for the breakdown powers are also plotted according to the  $K$  and  $K^2$  rules,  $P_{sc}/K$  and  $P_{sc}/K^2$ , respectively, where  $K$  is the number of carriers and  $P_{sc}$  is the single carrier breakdown power determined by the single-carrier nonstationary theory of [18]. FEST3D simulations are also included and labeled with “Num” tag.

TABLE V  
WORST CASE PREDICTION FOR KU-BAND SAMPLES. BREAKDOWN LEVELS ARE GIVEN IN POWER PER CARRIER.

Type	Gap (mm)	Sig.	20GCR		QS		FEST3D (W)
			(W)	$n_{gc}$	(W)	$n_{gc}$	
TF	0.14	6c	28.3	20	42.7	75	47.5
		6n	29.2	20	53.0	44	52.5
		8c	16.0	20	36.7	75	29.38
		8n	16.9	20	36.3	38	32.5
	0.42	6c	65.7	20	178.3	47	580
		6n	82.2	20	231.2	37	460
		8c	39.5	20	159.3	52	330
		8n	57.2	20	174.8	38	215
	0.64	6c	106.8	20	296.2	25	390
		6n	176.5	20	300.6	13	400
		8c	70.7	20	181.4	19	240
		8n	131.7	20	183.0	10	255
LP	0.14	6c	10.6	20	19.3	18	23.13
		6n	11.0	20	27.2	57	61.25
		8c	6.0	20	18.0	107	20
		8n	6.4	20	19.9	60	67.5
	0.42	6c	56.2	20	154.0	38	480
		6n	70.2	20	173.4	27	285
		8c	33.8	20	43.4	37	300
		8n	48.8	20	137.8	31	310
	0.64	6c	67.0	20	201.9	26	340
		6n	110.7	20	202.6	14	355
		8c	42.6	20	128.1	20	235
		8n	82.6	20	128.4	10	245
BP	1.31	6c	66.4	20	96.7	11	220
		6n	124.5	20	95.6	6	235
		8c	48.9	20	132.1	14	162.5
		8n	92.2	20	66.1	7	175

As it can be seen, the predicted breakdown power levels computed by the 20GCR are significantly lower (around 3 dB) than the QS method, which is closer to the  $K$  power curve.

The number of gap crossings is shown in Fig. 15. Whereas the number of gap crossings is obviously fixed to 20 for the 20GCR, the QS method yields a number of gap crossings that is different for each particular sample and signal having a great variation between cases. This is because each sample has a different SEY curve and work at a different  $f \times d$  product, and it is also expected that a different number of gap crossings is needed to produce a discharge.

The number of gap crossings predicted by the QS method start at a high value (100-200) for the 0.14 mm gap samples, and follow a decreasing trend as the gap increases, finishing below 20 for the largest gaps, i.e. for 0.64 mm and 1.31 mm.

Please note that a number of gap crossings of 100-200 for some of the results corresponding to the 0.14 mm gap samples, is not as excessive as it may appear. The frequency spacing yields a period of the envelope of 26.11 ns and 13.05 ns for the contiguous and non-contiguous channel frequency schemes, respectively. For a center frequency of around 12 GHz, this implies a number of cycles of 627 and 313, in one period of the envelope, for each of the two frequency schemes. Therefore, the 0.14 mm gap samples, working at a nominal multipactor order of  $n = 1$ , have a total of 627 and 313 gap crossings within a period of the envelope. In this case, a number of gap crossings of 100-200 implies only a  $T_{ON}$  of around a 16-32% and 32-64% of the total period  $T$ , respectively, for the two frequency schemes. Contrarily, 20 gap crossings yield a  $T_{ON}$

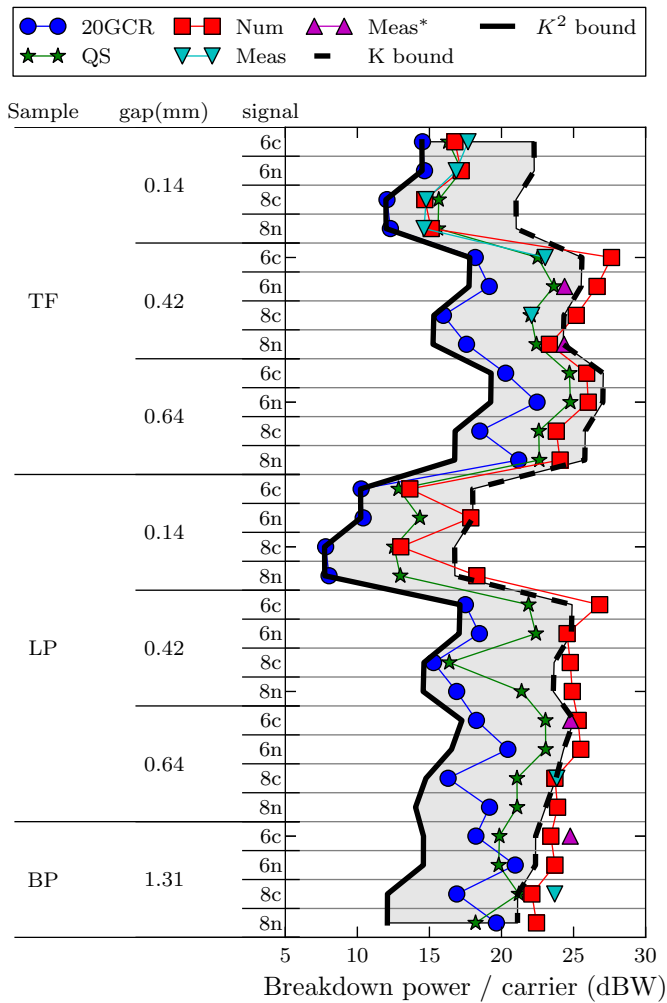


Fig. 14. Summary of breakdown threshold predictions and test results for Ku-band samples. FEST3D simulations are labeled with "Num" tag. Labels "c" and "n" stand for contiguous and non-contiguous frequency schemes. Breakdown levels are given in power per carrier. The minimum breakdown power of all tested phase configurations has been plotted with label "Meas". The maximum applied power for the cases where no multipactor has been observed has been also included with label "Meas\*".

of only 3-6% of the total envelope (approximately), which does in fact seem unrealistically low.

On the other hand, the 0.64 mm and 1.31 mm gap samples work at a nominal multipactor order of 5 and 7, respectively. In this case, a number of gap crossings of 10, for instance, implies around a 8-22% of the total envelope.

Table VI and Fig. 14 show the experimental results for some of the samples and frequency schemes of the project. Breakdown levels are given in power per carrier. Two measurements have been carried out for every phase condition. Numerical results computed with FEST3D (marked as F3 in the table) have been also included. There is missing data for some of the samples, either because they have not been tested yet or because no multipactor has been detected up to the maximum available power (around 300 W per channel) in the set up (marked as "ND" in the table). More testing is envisaged in the

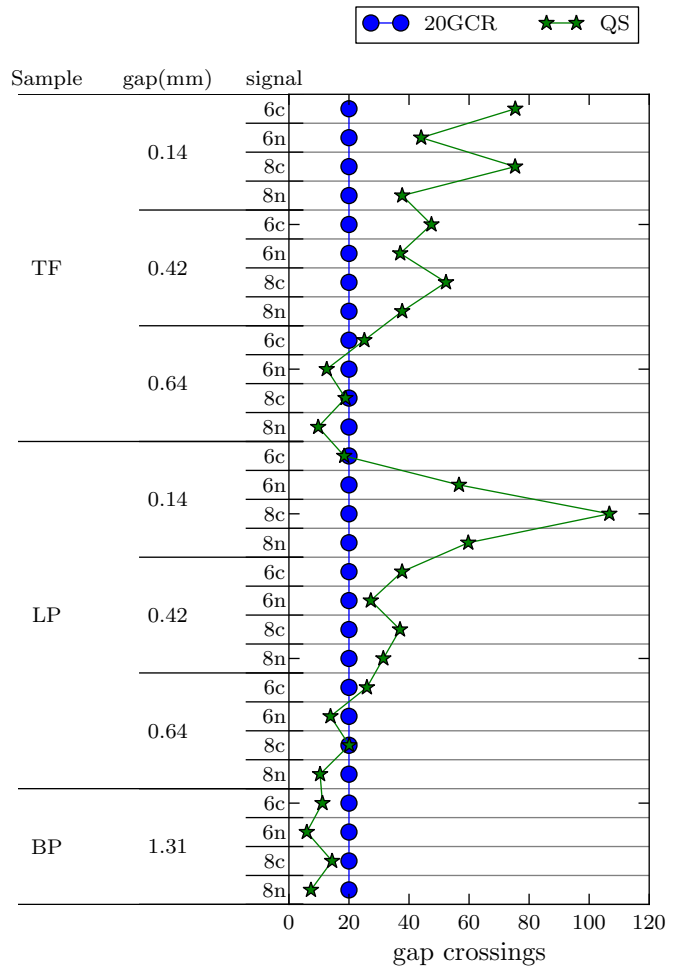


Fig. 15. Summary of the number of gap crossings of predictions for Ku-band samples.

future in order to have more comparison data. In Fig. 14, the minimum breakdown power of all tested phase configurations has been plotted with label "Meas" (corresponding to the definition of global error of Section VI-A). The maximum applied power for the cases where no multipactor has been observed has been also included with label "Meas\*".

It is worth noting that the experimental results are much closer to the QS predictions and to the FEST3D calculations than to the 20GCR predictions. The latter are in all cases much lower than the experimental results (around 3dB). As stated before, no extra margins have been applied to the predictions. This reveals that in fact the 20GCR seems to be very conservative, at least in the cases tested in this work.

Especially for large gaps, some FEST3D simulations yield a prediction above the theoretical  $K$  rule bound. This in principle may seem unrealistic, but remember that both the  $K^2$  and  $K$  bounds are computed assuming parallel-plates, which is indeed the worst case. In real structures, the effect of the non-homogeneous fields, finite geometry and high order modes contribute to increase the breakdown power with respect to the

TABLE VI  
EXPERIMENTAL RESULTS FOR THE KU-BAND SAMPLES. BREAKDOWN LEVELS ARE GIVEN IN POWER PER CARRIER.

Type	Gap (mm)	Sg.	Cd.	$\Phi_1$	$\Phi_2$	$\Phi_3$	$\Phi_4$	$\Phi_5$	$\Phi_6$	$\Phi_7$	$\Phi_8$	F3 (W)	M1 (W)	M2 (W)		
TF	6c	IP	QSn	x	0	0	0	0	0	0	0	x	47.5	59.6	58.6	
			FR	x	0	0	180	180	0	0	0	0	x	170	78	73
			FR	-	-	-	-	-	-	-	-	-	-	-	55.5	60
	6n	IP	QSn	x	0	0	0	0	0	0	0	0	x	52.5	53.5	51.8
			FR	x	0	0	180	180	0	0	0	0	x	78.8	89.5	89.5
			FR	-	-	-	-	-	-	-	-	-	-	-	49	48.5
	0.14	IP	QSn	0	0	0	0	0	0	0	0	0	0	29.4	30	30
			FR	0	350	331	299	299	331	350	0	0	0	39.4	61.5	59.5
			FR	-	-	-	-	-	-	-	-	-	-	-	32	32
	8c	IP	QSn	0	0	0	0	0	0	0	0	0	0	32.5	29	29
			FR	0	180	180	0	0	180	180	0	0	0	48.1	47.5	47.5
			FR	-	-	-	-	-	-	-	-	-	-	-	30.5	29.7
	6c	IP	QSn	x	0	0	0	0	0	0	0	0	x	580	ND	ND
			FR	x	0	180	0	0	180	0	0	0	x	700	ND	ND
			FR	-	-	-	-	-	-	-	-	-	-	-	205	201
	6n	IP	QSn	x	0	0	0	0	0	0	0	0	x	500	ND	ND
			FR	x	0	119	14	14	119	0	0	0	x	860	ND	ND
			FR	x	0	252	255	255	252	0	0	0	x	460	ND	ND
0.42	IP	QSn	0	0	0	0	0	0	0	0	0	0	330	ND	ND	
		FR	0	107	275	109	109	275	107	0	0	0	640	238	238	
		FR	-	-	-	-	-	-	-	-	-	-	-	164	162	
8c	IP	QSn	0	0	0	0	0	0	0	0	0	0	315	ND	ND	
		FR	0	127	133	132	132	133	127	0	0	0	490	ND	ND	
		FR	0	109	256	56	56	256	109	0	0	0	215	ND	ND	
8n	IP	QSn	x	0	0	0	0	0	0	0	0	x	340	-	-	
		FR	x	0	0	180	180	0	0	0	0	x	450	-	-	
		FR	-	-	-	-	-	-	-	-	-	-	-	ND	ND	
6n	IP	QSn	x	0	0	0	0	0	0	0	0	x	355	-	-	
		FR	x	0	0	180	180	0	0	0	0	x	470	-	-	
		FR	x	0	249	238	238	249	0	0	0	x	450	-	-	
LP 0.64	IP	QSn	0	0	0	0	0	0	0	0	0	0	235	-	-	
		FR	0	180	180	0	0	180	180	0	0	0	315	ND	ND	
		FR	0	238	237	238	238	237	238	0	0	0	355	-	-	
8c	IP	QSn	0	0	0	0	0	0	0	0	0	0	245	-	-	
		FR	0	180	180	0	0	180	180	0	0	0	320	-	-	
		FR	0	69	127	142	142	127	69	0	0	0	375	-	-	
6c	IP	QSn	x	0	0	0	0	0	0	0	0	x	220	-	-	
		FR	x	0	0	180	180	0	0	0	0	x	230	-	-	
		FR	x	0	105	123	123	105	0	0	0	x	225	-	-	
6n	IP	QSn	x	0	0	0	0	0	0	0	0	x	275	-	-	
		FR	x	0	0	180	180	0	0	0	0	x	245	-	-	
		FR	x	0	62	136	136	62	0	0	0	x	235	-	-	
BP 1.31	IP	QSn	x	0	0	0	0	0	0	0	0	x	190	-	-	
		FR	0	12	35	67	67	35	12	0	0	0	150	259	253	
		FR	0	56	125	141	141	125	56	0	0	0	163	-	-	
8c	IP	QSn	0	0	0	0	0	0	0	0	0	0	203	-	-	
		FR	0	180	0	180	180	0	180	0	0	0	185	-	-	
		FR	0	88	253	307	307	253	88	0	0	0	175	-	-	

parallel-plate approximation [28]. FEST3D takes into account all the previous effects, and that is the reason why some of the predictions for large gaps lie above the theoretical upper bound. In fact, this may be also the reason why, in the laboratory, some of the samples did not exhibit a multipactor discharge up to the maximum available power, even if the  $K$  bound lay below such maximum power.

#### D. Analysis of results

The average prediction error is presented in Table VII. The local error of the FEST3D numerical tool is also included for comparison.

TABLE VII  
AVERAGE PREDICTION ERROR FOR THE PREDICTION METHODS ON THE KU-BAND SAMPLES

	20GCR	QS	FEST3D
Local error (dB)	2.68	1.2	1.42
Global error (dB)	4.47	1.18	-

The analysis of the errors indicates that the 20GCR shows a considerable higher local and global error with respect to the QS method. The latter shows very good figures for both of them. This indicates that the QS method shows the best prediction performance and, again, that the 20GCR is very conservative (more than 4 dB).

The local error of the FEST3D simulations show similar values than for the QS method. This is because the designed samples are waveguides with long irises in order to resemble the parallel plate case as much as possible. With other more complicated geometries involving fringing field effects, numerical full-wave EM solvers such as FEST3D are expected to give more realistic results.

## VII. CONCLUSIONS

It is clear from the experimental results that the new QS prediction technique offers better predictions than the 20GCR. This fact was expected since the former uses a more sophisticated theoretical background based on multipactor physics. Moreover, for the prediction the QS method considers the frequency scheme and the SEY curve of the coating material for each specific case, offering more accuracy and versatility with respect to the 20GCR.

Besides being more precise, the predicted breakdown power levels of the QS technique are significantly higher than the ones provided by the 20GCR. This is an important factor for the industry because this would allow increasing the operating power of the devices, thus reducing the designs constraints and increasing the margins.

Finally, the QS method may use pre-calculated multipactor maps, in order to predict the worst case without having to implement any multipactor theory or use any multipactor numerical software.

## ACKNOWLEDGMENT

The authors would like to thank Isabel Montero and Luis Galan of the Consejo Superior de Investigaciones Cientificas (CSIC) and the Universidad Autonoma de Madrid (UAM), respectively, for conducting the SEY measurements reported in Section IV-D. Thanks to ESA/ESTEC for having funded this research activity through the Contract "RF Breakdown in Multicarrier Systems" (1-9918/06/NL/GLC), and to the Ministerio de Ciencia e Innovacion (Spain) for the support through the "Programa Torres Quevedo" PTQ06-2-0693.

## REFERENCES

- [1] E. W. B. Gill and A. von Engel, "Starting potentials of high-frequency gas discharges at low pressure," *Proceedings of the Royal Society of London, Series A, Mathematical and Physical Sciences*, vol. 192, no. 1030, pp. 446-463, Feb. 1948.

- [2] A. Hatch and H. Williams, "The secondary electron resonance mechanism of low-pressure high-frequency gas breakdown," *Journal of Applied Physics*, vol. 25, no. 4, pp. 417–423, Apr. 1954.
- [3] J. Vaughan, "Multipactor," *IEEE Trans. Electron Devices*, vol. 35, pp. 1172–1180, Jul. 1988.
- [4] P. Farnsworth, "Television by electron image scanning," *Journal of the Franklin Institute*, vol. 218, no. 4, pp. 411–444, Oct. 1934.
- [5] R. J. Cameron, R. Mansour, and C. M. Kudsia, *Microwave Filters for Communication Systems: Fundamentals, Design and Applications*. John Wiley & Sons, 2007.
- [6] R. Geng, P. Goudket, R. Carter, S. Belomestnykh, H. Padamsee, and D. Dykes, "Dynamical aspects of multipacting induced discharge in a rectangular waveguide," *Nuclear Instruments and Methods in Physics Research Section A: Accelerators, Spectrometers, Detectors and Associated Equipment*, vol. 538, no. 1-3, pp. 189 – 205, 2005.
- [7] C. Vicente, M. Mattes, D. Wolk, H. L. Hartnagel, J. R. Mosig, and D. Raboso, "FEST3D: A simulation tool for multipactor prediction," in *Proceedings of the 5th International Workshop on Multipactor, RF and DC Corona and Passive Intermodulation in Space RF Hardware*. ESTEC, Noordwijk, The Netherlands, Sept. 12-14 2005, pp. 11–17.
- [8] "FEST3D Full-wave Electromagnetic Simulation Tool," <http://www.fest3d.com/>.
- [9] "SPARK3D Multi-format High Power Simulation Tool," <http://www.fest3d.com/>.
- [10] "CST Computer Simulation Technology Center," <http://www.cst.de/>.
- [11] K. H. Geisser and D. Wolk, "Multipactor testing of multiplexer and waveguide components exposed to multiple carrier loading," in *Proceedings of the 2nd International Workshop on Multipactor, RF and DC Corona and Passive Intermodulation in Space RF Hardware*. ESTEC, Noordwijk, The Netherlands, Mar. 12-13 1996.
- [12] N. Rozario, H. F. Lenzing, F. Reardon, M. S. Zarro, and C. G. Baran, "Investigation of Telstar 4 spacecraft Ku-band and C-band antenna components for multipactor breakdown," *IEEE Transactions on Microwave Theory and Techniques*, vol. 42, no. 4, pp. 558–564, Apr. 1994.
- [13] S. Anza, M. Mattes, C. Vicente, J. Gil, D. Raboso, V. E. Boria, and B. Gimeno, "Multipactor theory for multicarrier signals," *Physics of Plasmas*, vol. 18, no. 3, p. 032105, 2011.
- [14] S. Anza, C. Vicente, D. Raboso, J. Gil, B. Gimeno, and V. E. Boria, "Enhanced Prediction of Multipaction Breakdown in Passive Waveguide Components including Space Charge Effects," in *IEEE International Microwave Symposium*, Atlanta, USA, Jun 2008, pp. 1095–1098.
- [15] ECSS, "Multipactor Tool," <http://www.aurorasat.es/multipactortool.php>.
- [16] *Space Engineering: Multipacting Design and Test*. ESA Publication Division, The Netherlands, May 2003, vol. ECSS-20-01A, edited by ESA-ESTEC.
- [17] A. Woode and J. Petit, "Diagnostic investigations into the multipactor effect, susceptibility zone measurements and parameters affecting a discharge," ESTEC working paper No. 1556, Noordwijk, Tech. Rep., Nov. 1989.
- [18] S. Anza, C. Vicente, J. Gil, V. E. Boria, B. Gimeno, and D. Raboso, "Nonstationary statistical theory for multipactor," *Physics of Plasmas*, vol. 17, no. 6, p. 062110, June 2010.
- [19] A. G. Sazontov, V. A. Sazontov, and N. K. Vdovicheva, "Multipactor breakdown prediction in a rectangular waveguide: statistical theory and simulation results," *Contributions to Plasma Physics*, vol. 48, no. 4, pp. 331–346, May 2008.
- [20] D. Wolk, D. Schmitt, and T. Schlipf, "A novel approach for calculating the multipaction threshold in multicarrier operation," in *Proceedings of the 3rd International Workshop on Multipactor, RF and DC Corona and Passive Intermodulation in Space RF Hardware*. ESTEC, Noordwijk, The Netherlands, Sept. 4-6 2000, pp. 85–91.
- [21] J.-C. Angevain, L. Drioli, P. Delgado, and C. Mangenot, "A boundary function for multicarrier multipaction analysis," in *Antennas and Propagation, 2009. EuCAP 2009. 3rd European Conference on*, march 2009, pp. 2158 –2161.
- [22] S. Anza, C. Vicente, B. Gimeno, V. E. Boria, and J. Armendariz, "Long-term multipactor discharge in multicarrier systems," *Physics of Plasmas*, vol. 14, no. 8, pp. 082112–082112–8, Aug. 2007.
- [23] S. Anza, M. Mattes, J. Armendariz, J. Gil, C. Vicente, B. Gimeno, V. Boria, and D. Raboso, "RF breakdown prediction for microwave passive components in multi-carrier operation," in *Ultra-Wideband, Short Pulse Electromagnetics 9*, F. Sabath, D. Giri, F. Rachidi, and A. Kaelin, Eds. Springer New York, 2010, pp. 375–381.
- [24] S. Kirkpatrick, C. D. Gelatt, and M. P. Vecchi, "Optimization by simulated annealing," *Science*, vol. 220, no. 4598, pp. 671–680, 1983.
- [25] K. Price, R. M. Storn, and J. A. Lampinen, *Differential Evolution: A Practical Approach to Global Optimization*. Springer, 2005.
- [26] "ANSYS HFSS," <http://www.ansys.com/>.
- [27] K. S. Parikh, D. K. Singh, A. P. Kumar, M. S. Rusia, and M. K. Sangeetha, "Multi-carrier multipactor analysis of high power antenna Tx-Tx diplexer for Satcom applications," in *Proceedings of the 4th International Workshop on Multipactor, RF and DC Corona and Passive Intermodulation in Space RF Hardware*. ESTEC, Noordwijk, The Netherlands, Sept. 8-11 2003, pp. 435–441.
- [28] V. E. Semenov, E. I. Rakova, D. Anderson, M. Lisak, and J. Puech, "Multipactor in rectangular waveguides," *Physics of Plasmas*, vol. 14, no. 3, p. 033501, 2007.



**Sergio Anza** was born in Madrid, Spain, in 1978. He received the B.S. degree in telecommunications engineering in 2002 from the Universidad Politécnica de Valencia, Spain, and the M.S. degree in aerospace science and technology in 2006 from the Universitat Politècnica de Catalunya, Barcelona, Spain. He is currently working toward the Ph.D. degree in the Communications Department of the Universidad Politécnica de Valencia, Spain.

From 2003 to 2006 he joined the Consejo Superior de Investigaciones Científicas (CSIC), of the Spanish Ministry of Science. Since 2007, he is with Aurora Software and Testing S.L. His current research interests include the areas of theory and numerical techniques for the modeling and prediction of non-linear phenomena in RF high power devices for space applications, with special emphasis on the study of the multipactor effect appearing in power microwave subsystems.



**Carlos Vicente** (M08) was born in Elche, Spain, in 1976. He received the Dipl. degree in Physics from the Universidad de Valencia, Valencia, Spain, in 1999, and the Dr.-Ing degree in Engineering from the Technical University of Darmstadt, Darmstadt, Germany, in 2005.

From 1999 to the beginning of 2001, he was a Research Assistant with the Department of Theoretical Physics, Universidad de Valencia. From 2001 to 2005, he was a Professor Assistant with the Institute of Microwave Engineering, Technical University of Darmstadt. Since 2005, he has been with the Microwave Applications Group, Universidad Politécnica de Valencia, Valencia, Spain. In 2006, he co-founded Aurora Software and Testing S. L., which is devoted to the telecommunications sector. He is currently the Technical Director of the company.

His research concerns the analysis and design of passive components for communications satellites with a special emphasis on high-power practical aspects such as passive intermodulation, corona discharge, and multipaction.



**Jordi Gil** (M08) was born in Valencia, Spain, in 1977. He received the Licenciado degree in Physics from the Universidad de Valencia, Valencia, Spain, in 2000, and the Ph.D. degree in Telecommunications Engineering from the Universidad Politécnica de Valencia, Valencia, Spain, in 2010.

From 2001 to 2004, he was Researcher with the Aerospaziale Italian Company, Ingegneria Dei Sistemi-S.p.A., under the frame of the V European Framework Programme. From 2004 to 2006, he joined the Microwave Applications Group, Universidad Politécnica de Valencia, in the frame of a European reintegration grant funded by the VI European Framework Programme. In 2006 he cofounded the company Aurora Software and Testing S.L., devoted to the space sector. He is currently the Managing Director of the company where he also continues his research activities.

His current research interests include numerical methods in computer-aided techniques for the analysis of microwave and millimeter passive components based on waveguide technology, and nonlinear phenomena appearing in power microwave subsystems for space applications.



**Michael Mattes** received the Diplom-Ingenieur degree from the University of Ulm, Ulm, Germany, in 1996, and the Ph.D. degree from the Ecole Polytechnique Fdrale de Lausanne (EPFL), Lausanne, Switzerland, in 2003. Following one year as a Research Fellow with the Department of Microwave Techniques, University of Ulm, in September 1997, he joined the Laboratory of Electromagnetism and Acoustics (LEMA), Ecole Polytechnique Fdrale de Lausanne (EPFL). He was responsible for the development and implementation of the Full-wave Electromagnetic Simulation Tool (FEST), version 3.0, within the framework of the European Space Agency (ESA) project Integrated computer-aided design (CAD) tool for waveguide components (ESA/European Space Research and Technology Centre (ESTEC) 12 465/97/NL/NB). He was and is involved in many EU, ESA and Swiss research projects. His research interests include electromagnetic theory in a multi-disciplinary framework, related numerical techniques, and microwave filters.



**Dieter Wolk** was born in Wilhelmshaven, Germany, in August 1948. He received the Dipl. Ing. degree in electrical engineering (RF technique) from the Technical University of Hannover, Germany, in 1975.

He joined the Radio Link Division of AEG-Telefunken, Backnang, Germany, where he was involved in the development of solid state power amplifiers (Gunn, IMPATT, FET). Since 1979 he has been with the Space Communications System Division of AEG-Telefunken, now Tesat Spacecom GmbH & Co. KG, Backnang, Germany. Currently he is Senior Engineer in the passive RF equipment division and engaged in research and development of advanced filters, multiplexers and passive components for space application. His special research interest includes non-linear effects in passive high power devices (multipactor, corona and passive intermodulation).



**Ulrich Wochner** was born 1968 in Germany. After obtaining his Degree in Physics he joined Tesat Spacecom GmbH & Co. KG, Backnang, Germany, in 2001, as RF-Engineer in the Tesat Test Facility, where he was focused on high power testing. Since 2004 he is responsible for RF - Components at the RF-Engineer Development Department.



**Vicente E. Boria** (S91-A99-SM02) was born in Valencia, Spain, on May 18, 1970. He received his Ingeniero de Telecomunicacin degree (with first-class honors) and the Doctor Ingeniero de Telecomunicacin degree from the Universidad Politcnica de Valencia, Valencia, Spain, in 1993 and 1997, respectively.

In 1993 he joined the Departamento de Comunicaciones, Universidad Politcnica de Valencia, where he has been Full Professor since 2003. In 1995 and 1996, he was holding a Spanish Trainee position with the European Space Research and Technology Centre, European Space Agency (ESTEC-ESA), Noordwijk, The Netherlands, where he was involved in the area of EM analysis and design of passive waveguide devices. He has authored or co-authored 7 chapters in technical textbooks, 75 papers in refereed international technical journals, and over 150 papers in international conference proceedings. His current research interests are focused on the analysis and automated design of passive components, left-handed and periodic structures, as well as on the simulation and measurement of power effects in passive waveguide systems.

Dr. Boria has been a member of the IEEE Microwave Theory and Techniques Society (IEEE MTT-S) and the IEEE Antennas and Propagation Society (IEEE AP-S) since 1992. He is member of the Editorial Boards of the IEEE Transactions on Microwave Theory and Techniques, IEEE Microwave and Wireless Components Letters, Proceeding of the IET (Microwaves, Antennas and Propagation), IET Electronics Letters and Radio Science. He is also a member of the Technical Committees of the IEEE-MTT International Microwave Symposium and of the European Microwave Conference.



**Benito Gimeno** (M01) was born in Valencia, Spain, on January 29, 1964. He received the Licenciado degree in Physics in 1987 and the PhD degree in 1992, both from the Universidad de Valencia, Spain. He was a Fellow at the Universidad de Valencia from 1987 to 1990. Since 1990 he served as Assistant Professor in the Departamento de Fsica Aplicada y Electromagnetismo and ICMUV (Instituto de Ciencia de Materiales) at the Universidad de Valencia, where he became Associate Professor in 1997 and Full Professor in 2010. He was working

at ESA/ESTEC (European Space Research and Technology Centre of the European Space Agency) as a Research Fellow during 1994 and 1995. In 2003 he obtained a Fellowship from the Spanish Government for a short stay at the Universita degli Studi di Pavia (Italy) as a Visiting Scientific. His current research interests include the areas of computer-aided techniques for analysis of microwave and millimetre-wave passive components for space applications, waveguides and cavities structures including dielectric objects, electromagnetic band-gap structures, frequency selective surfaces, and non-linear phenomena appearing in power microwave subsystems and particle accelerators (multipactor effect, corona effect and passive inter-modulation phenomena).



**David Raboso** was born in Alcazar de San Juan, Spain 1967. He received his Master Degree in Physics at the University Autonoma of Madrid in 1992. The same year started working at the European Space Agency in the field of RF breakdown and Passive Intermodulation. In 2001 David completed a Master in Space Engineering with University of Delft (Netherlands).

Presently, he is Chairman of European Networks and ECSS Working Groups in Multipactor effect, Corona, RF high power and PIM. He is also responsible for the R& D and testing services area in RF breakdown at ESA. David Raboso has participated in the organization of every MULCOPIM workshop since 1993 and in 2003 became organizer chairman of the event. Since 2010, David Raboso is manager of the European high power RF laboratory based in Valencia (Spain).